



# A simple and low-cost triboelectric nanogenerator based on two dimensional ZnO nanosheets and its application in portable electronics

P. Supraja<sup>a</sup>, R. Rakesh Kumar<sup>a,\*</sup>, Siju Mishra<sup>a</sup>, D. Haranath<sup>a</sup>, P. Ravi Sankar<sup>b</sup>, K. Prakash<sup>b</sup>, N. Jayarambabu<sup>a</sup>, T. Venkatappa Rao<sup>a</sup>, K. Uday Kumar<sup>a</sup>

<sup>a</sup> Energy Materials and Devices Lab, Department of Physics, National Institute of Technology, Warangal 506004, India

<sup>b</sup> Flexible Electronics Lab, Department of Electronics and Communication Engineering, National Institute of Technology, Warangal 506004, India

## ARTICLE INFO

### Article history:

Received 8 September 2021

Received in revised form 15 December 2021

Accepted 3 January 2022

Available online 7 January 2022

### Keywords:

Energy harvesting

Triboelectric nanogenerators

Contact electrification

ZnO nanosheets

Polyethylene terephthalate (PET)

Self-powered system

## ABSTRACT

The exploration of new triboelectric materials is considered a significant research area to reduce the cost and complexity of the triboelectric nanogenerator (TENG) device and improve its energy conversion efficiency. In this report, a new triboelectric material pair has been demonstrated to prepare an inexpensive and high-performance TENG. A low-cost hot plate-assisted hydrothermal process is used to prepare the ZnO nanosheets on an aluminum substrate. TENG is made using ZnO nanosheet film, PET/ITO, and operates in vertical contact separation mode. The proposed TENG generates electricity through contact electrification and electrostatic induction. The fabricated TENG is tested for the switching polarity test and confirmed the output voltage generated by TENG alone. The TENG can deliver an open-circuit voltage and short-circuit current of  $\sim 4.9$  V and  $10 \mu\text{A}$ , respectively, for repeated hand tapping.

Further, the performance of the proposed TENG is tested under resistive loads, and the maximum power density of  $1 \mu\text{W}/\text{cm}^2$  observed at a load resistance of  $5 \text{ M}\Omega$ . Similarly, TENG is also tested under capacitive loads and found the maximum energy stored value of  $16.9 \mu\text{J}$  at the load capacitance of  $47 \mu\text{F}$ . In addition, the effect of different frequencies of the applied force and device size on the TENG response is studied. The TENG can light up 3 LEDs instantaneously and power the digital watch and 24 LEDs using an energy storage element. The present TENG shows a low-cost and straightforward process and can harvest energy from low-frequency bio-mechanical vibrations. The proposed TENG has potential applications in self-powered electronic devices and systems.

© 2022 Elsevier B.V. All rights reserved.

## 1. Introduction

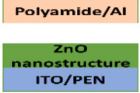
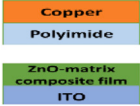

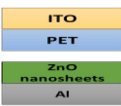
With the rapid advances in portable electronic devices and Internet of Things (IoT) devices, the demand for energy harvesting has been dramatically increasing [1,2]. These devices presently work with conventional batteries. However, conventional batteries have limited battery life, bulky packaging, rigid frames, and are not environmentally friendly [3,4]. In some cases, battery replacement at inaccessible environments is difficult and expensive. In other cases, such as implantable medical devices, battery replacement requires additional surgery and risks the patient's life [3,4]. Therefore, the development of efficient, renewable, eco-friendly, and sustainable energy sources is essential to power portable electronic devices [5].

Several energy harvesting technologies such as photovoltaics, piezoelectric, triboelectric, thermoelectric, electromagnetic have been developed to provide power to portable electronic devices. The triboelectric energy harvesting phenomenon has many advantages over other methods [6,7]. The triboelectric nanogenerator (TENG) technology is considered suitable for self-powered electronic devices. It has attracted much research interest due to its high output voltage and current with simple structures and easier packaging than piezoelectric nanogenerators. The TENG device fabrication has a broad choice of materials, and new materials are still being added [7–10]. In addition, TENG could convert almost all forms of mechanical energy such as vibration, rotation, force, pressure, airflow, water flow, raindrops into electricity [6]. TENG can convert both low and high-frequency vibrations into electricity [5,11]. In TENG's, the cyclic contact and the separation between different materials create a potential difference due to contact electrification and electrostatic induction [12]. Further, TENG can be operated in four modes: sliding, single electrode, free-standing, and contact-separation [13–16].

\* Corresponding author.

E-mail address: [rakeshr@nitw.ac.in](mailto:rakeshr@nitw.ac.in) (R.R. Kumar).

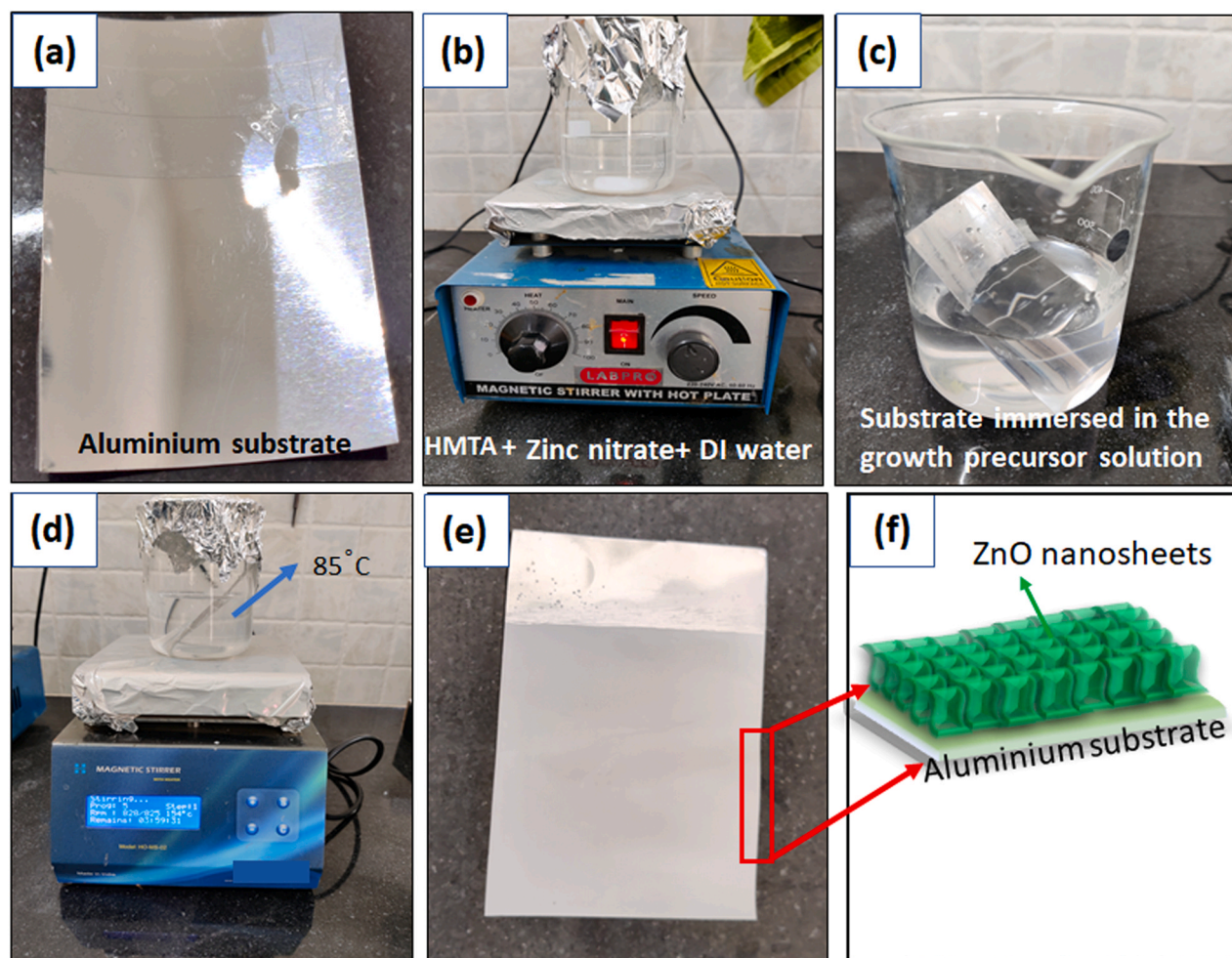
**Table 1**  
Literature review of TENG's based on ZnO nanostructures.

Sl.no	Device structure	Friction materials	Output performance	References
1		ZnO nano ripples /polyimide	Output Voltage-80 V, Current-0.82 $\mu$ A Load resistance- not available	[25]
2		Polyamide/ZnO nanostructure	Output Voltage-20 V, Current-1.36 $\mu$ A Load resistance- not available	[26]
3		Polyimide/ZnO matrix composite film	Output Voltage-105 V (Load resistance-100 M $\Omega$ ) Power density-2.5 W/m <sup>2</sup> (Load resistance-5 M $\Omega$ )	[27]
4		Polyimide/Al doped ZnO	Output Voltage- 98.4 V (Load resistance-120 M $\Omega$ ), Current-8.33 $\mu$ A	[28]
5		PDMS/Sb-doped ZnO nanorods	Output Voltage-12 V, Current density-0.11 $\mu$ A/cm <sup>2</sup> Load resistance- not available	[29]
6		PDMS/ZnO micro balloon/PTFE	Output Voltage-57 V (Load resistance-100 M $\Omega$ ) Power density-1105 mW/m <sup>2</sup> (Load resistance-2 M $\Omega$ )	[30]
7		ZnO nanorods/PDMS	Output Voltage-3.62 V, Current - 112.7 nA Load resistance- not available	[31]
8		Ag nanowires+ZnO nanotubes+PDMS/Al	Output Voltage-350 V (Load resistance-50 M $\Omega$ ) Power density-1.1 mW/cm <sup>2</sup> (Load resistance-20 M $\Omega$ )	[32]
9		PET/ZnO+PDMS	Output Voltage-3.5 V (Load resistance-100 M $\Omega$ ) Power density-4.8 $\mu$ W/cm <sup>2</sup> (Load resistance-70 M $\Omega$ )	[33]
10		Kapton/ZnO-Polystyrene	Output Voltage-7 V, Power density-0.23 mW/m <sup>2</sup> Load resistance- not available	[34]
11		PET/ZnO nanosheets	Output Voltage ~ 4.5 V (Load resistance-20 M $\Omega$ ) Current ~ 10 $\mu$ A Power ~ 25 $\mu$ W (Load resistance-5 M $\Omega$ )	Present work

Among the four working modes of TENG, contact separation mode is simple and easy to make and test the device. The performance of TENG is good in contact-separation mode with high power densities compared to the other modes [17,18]. In addition, the physical damage to the tribo layers is less in contact separation mode than the lateral sliding and free-standing mode. TENG's vertical contact separation mode generally lasts longer due to lesser friction damage. Therefore, TENG's vertical contact separation mode is selected in this manuscript.

Due to the rapid growth of flexible TENGs, many research groups focused on improving the TENGs performance through a new

material synthesis, advanced structural designs, mechanical-coupling effects [19,20]. However, the new triboelectric materials exploration is still a significant research area to reduce the cost and complexity of the TENG device and enhance its energy conversion efficiency. In this manuscript, ZnO nanosheet film and polyethylene terephthalate (PET) were used for the first time as a new triboelectric pair in TENG design. The present study is the first report on TENG-based on ZnO nanosheets and PET to the best of our knowledge. In this manuscript, ZnO nanosheets synthesized directly on aluminum substrate, PET side of ITO/PET were used as friction layers, eliminating the need to attach the electrodes or depositing



**Fig. 1.** ZnO nanosheet networks synthesis procedure, (a) clean aluminum substrate, (b) ZnO nanosheet growth solution preparation, (c) aluminum substrate is immersed ZnO growth precursor solution, (d) ZnO nanosheet film synthesis on a hot plate at 85°C growth solution temperature, (e) ZnO thin film on aluminum substrate, (f) schematic of ZnO nanosheets on aluminum.

electrodes. However, there were reports on TENGs based on ZnO nanorods, ZnO nanowires, ZnO nanolayers, and ZnO nanoripples, but not on ZnO nanosheets. The literature review of all the TENGs based on ZnO nanostructures and the results are summarized in terms of the device structure, friction layers, output performance is presented in Table 1. The ZnO is a very promising material, and it has several advantages like non-toxic, cost-effective, bio-compatible, environmentally friendly, and excellent stability [21]. Further, ZnO nanosheets synthesis has several advantages: simple, low cost, rapid growth, seed layer-free, single-step procedure compared to multi-step and seed layer assisted ZnO nanorods and nanowires [22,23]. In addition, ZnO nanosheets growth is directly obtained on Aluminum substrate. Therefore, the substrate acts as one conducting electrode for the TENG device and reduces the fabrication steps. Furthermore, the mechanical strength of the ZnO nanosheets is more than nanorods; as a result, the device can withstand high-value forces and produce electrical energy [24].

In this manuscript, TENG is fabricated for the first time with ZnO nanosheet film and PET as a novel triboelectric pair for harvesting mechanical energy. The TENG response was studied under load resistance and load capacitance to determine the maximum power and energy generated. In addition, fabricated TENG has been demonstrated for powering the digital watch, 24 LEDs with the help of charged capacitors. Finally, with bio-mechanical energy and tapping machines, TENG stability was tested over many test cycles.

## 2. Experimental

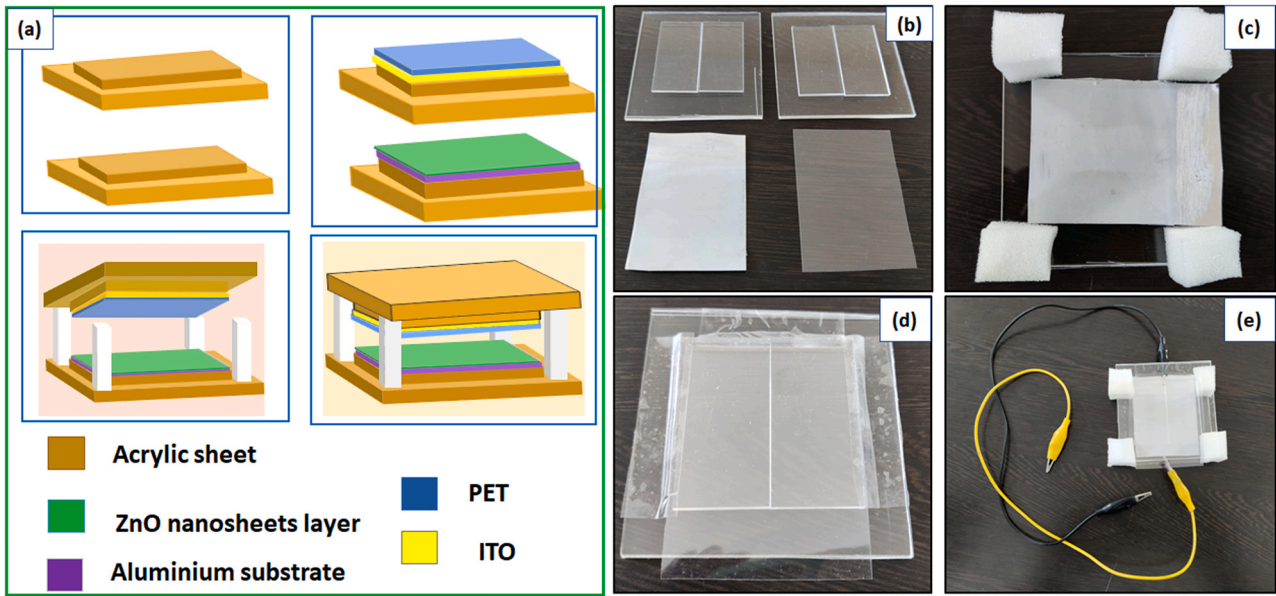
### 2.1. Materials

Zinc nitrate hexahydrate and hexamethylenetetramine (HMTA) and ITO coated PET (60  $\Omega$ /sq) sheets were obtained of Sigma Aldrich. Aluminum foils of thickness  $\sim 79.84 \mu\text{m}$  were obtained from Special metals Pvt. Ltd (See [Supplementary information](#) (SI), S1). Acrylic sheets, cardboard, sponges were brought from the local market.

### 2.2. Synthesis of ZnO nanosheets on aluminum substrate

The original photographs of the different steps of the synthesis process for ZnO nanosheets using the hot-plate assisted hydrothermal method are shown in Fig. 1(a)–(e). The synthesis procedure of ZnO nanosheets is similar to our previous report [35].

First, Zinc nitrate hexahydrate and HMTA were dissolved in 100 ml of de-ionized (DI) water for each precursor in a separate beaker and stirred for 15 min at room temperature. In the next step, two solutions were mixed, and the resulting solution was stirred for 20 min to get a clear solution. The aluminum substrate was covered with cello tape on one side to avoid double-sided coating during the synthesis. Next, the aluminum substrate was placed in a growth precursor solution, sealed with food packaging aluminum foil as shown in Fig. 1(d), and the beaker was kept on the hot plate at a



**Fig. 2.** (a) Schematic of the TENG fabrication steps, real-time images of TENG device fabrication steps (b) acrylic base sheets, ZnO film, ITO/PET films, (c) ZnO nanosheet film on aluminum attached to one of the acrylic bases, (d) ITO/PET substrate attached to another acrylic base with PET side facing up, (e) final TENG device with electrode connection for response measurement.

growth solution temperature of 85°C for 4 h. After 4 h of growth, the growth solution beaker was cooled to room temperature, and aluminum substrate was removed from the solution and cleaned with DI water. The white-coated region that appeared on the aluminum substrate shown in Fig. 1(e) indicates the ZnO thin film formation on the aluminum substrate.

### 2.3. Fabrication of TENG device

In this work, the ZnO nanosheets network film and PET surface of PET/ITO substrate were the two dielectric materials used to fabricate the TENG device. The ITO surface and the aluminum substrate acted as TENG's top and bottom electrodes, respectively. The schematic of the device fabrication is shown in Fig. 2(a). The actual pictures of the final TENG device and different fabrication steps are shown in Fig. 2(b)–(e). Initially, ZnO coated aluminum substrate with the aluminum side firmly attached to the acrylic sheet of the selected dimension by scotch tape with ZnO nanosheets film facing up like shown in Fig. 2(c).

Similarly, PET/ITO substrate with ITO side attached to another acrylic sheet firmly by scotch tape with PET surface facing up like shown in Fig. 2(d). Then, all corners of the lower acrylic sheet were attached with sponge spacers with the application of a strong adhesive. Next, another acrylic sheet with PET/ITO was placed over the spacer and attached with a strong adhesive. Due to the sponge spacer, a finite gap (1.2 cm) exists between the lower ZnO nanosheet film and the upper PET surface. Finally, two electrode lead wires were connected from the ITO side and the aluminum side to measure the TENG electrical output, as shown in Fig. 2(e).

Initially, TENG (5 × 5 cm<sup>2</sup>) was fully characterized with a distance of 1.2 cm between tribo layers and a hand tapping frequency of ~3–4 Hz. Then, the same TENG response was tested with different frequencies of hand tapping to check the frequency response. Finally, TENG was demonstrated for powering the digital watch, switching on commercial LEDs. In addition, TENGs with different device sizes of 5 × 5, 4 × 4, 3 × 3, 2 × 2 cm<sup>2</sup> were fabricated and tested their response with fixed space between tribo layers and applied force

frequency. Finally, the TENG stability was tested over many cycles using hand tapping, linear motor, and sewing machine.

### 2.4. Characterization and measurements

The surface morphology of ZnO thin film and PET was investigated using a scanning electron microscope (SEM, VEGA3 TESCAN). The crystallinity of the ZnO thin film and PET surface was studied by X-ray diffraction (XRD, Bruker D8). The output voltage from TENG against hand tapping was recorded using a digital oscilloscope (Tektronix TBS1102) with the aid of interface software (Tekvisa) to the computer. The short-circuit current of TENG was measured with an in-house-assembled current preamplifier (CNI570) [36–39] (SI, S2).

## 3. Results and discussion

### 3.1. Scanning electron microscopy (SEM)

The surface morphology of the ZnO thin film and the PET surface of PET/ITO are shown in Fig. 3(a) and (b). Fig. 3(a) confirms the vertically grown ZnO nanosheets on the substrate with uniform density and connectivity among them (SI, S3). The obtained nanosheets produce a rough topography for ZnO thin film. The SEM image in Fig. 3(b) confirms that the PET surface appears smooth compared to ZnO nanosheet film. Further XRD studies confirm the crystalline nature of the ZnO nanosheet film and the PET surface. The XRD pattern of the ZnO thin film is shown in Fig. 3(c), and all the ZnO diffraction peaks were indexed with red color. The ZnO diffraction peaks were in good agreement with the JCPDS card no. 751526 [40]. Similarly, all the diffractions peaks of the aluminum substrate were indexed in blue color and agreed well with JCPDS card no. 040787. In addition, the additional diffraction peaks observed at 20.4°, 60.5° were assigned to the ZnAl: layered double hydroxide (LDH) layer that was formed between the ZnO nanosheets and the aluminum substrate [41,42]. The intense diffraction peak

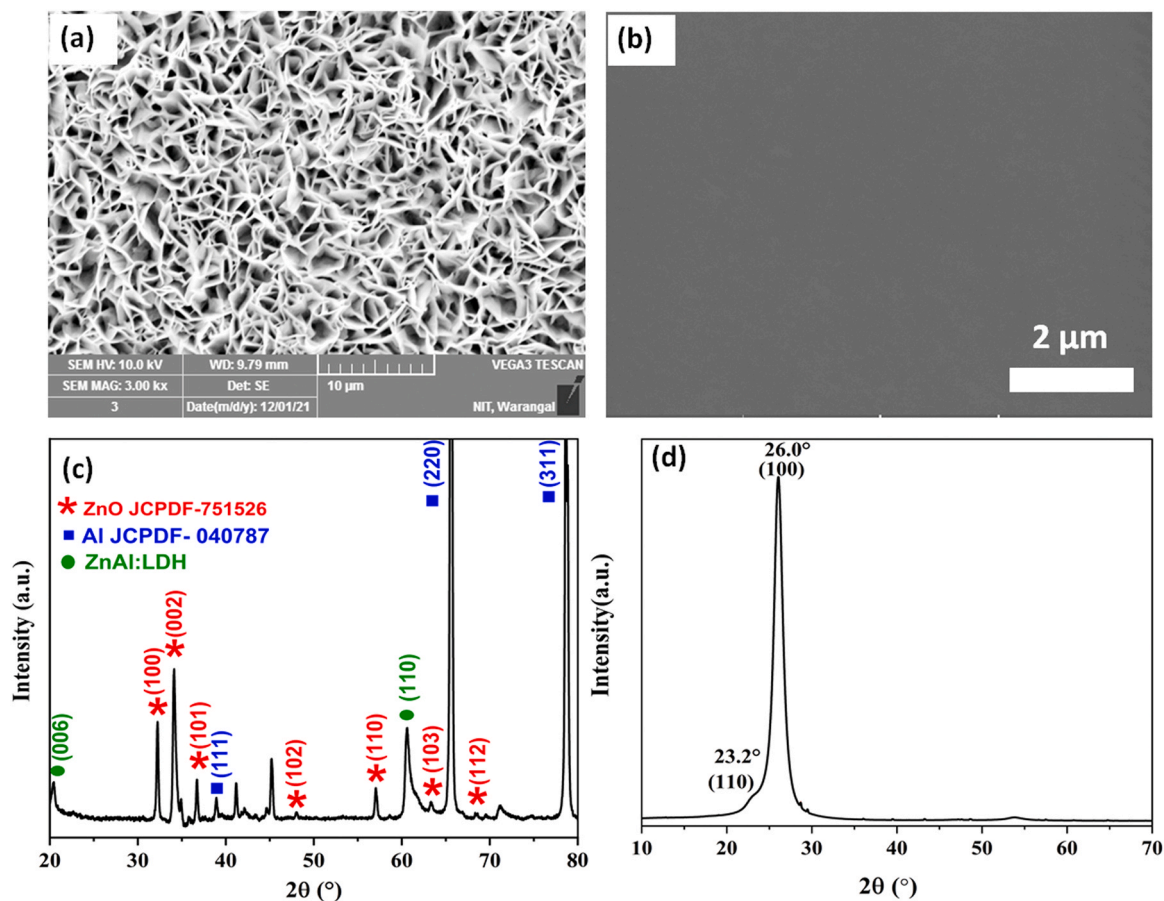


Fig. 3. SEM images of (a) ZnO nanosheets, (b) PET surface, XRD pattern of (c) ZnO nanosheet film, (d) PET surface.

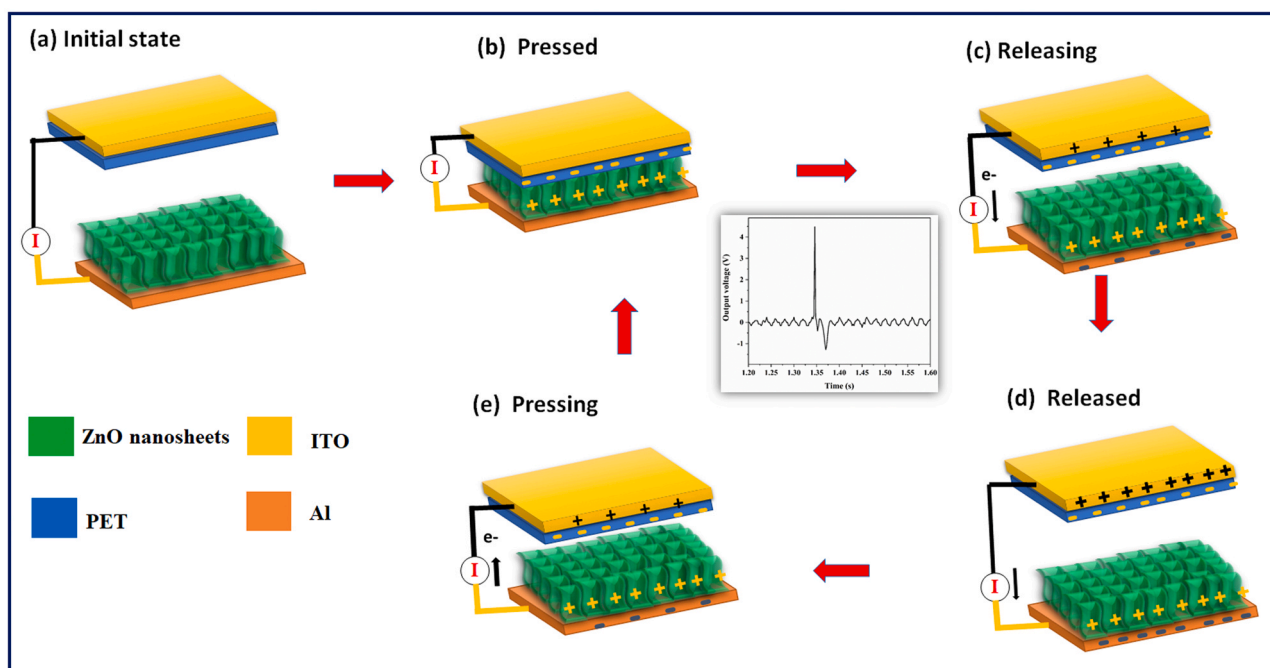
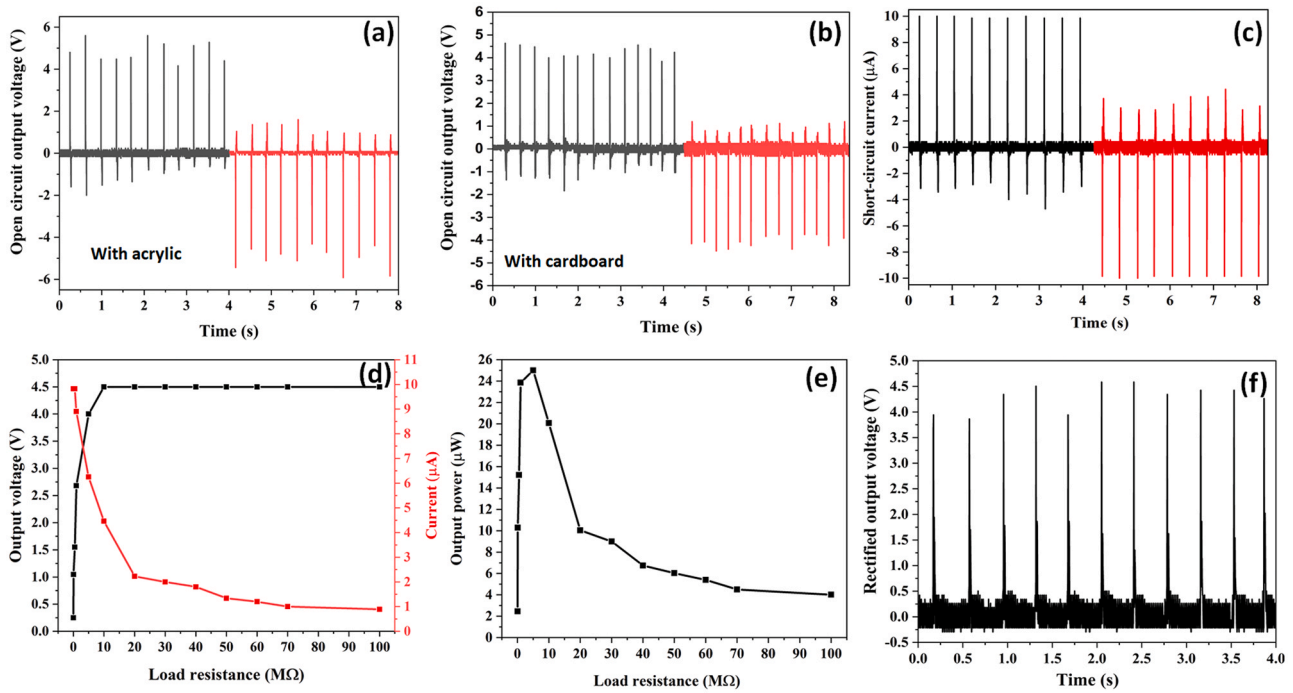


Fig. 4. Schematic illustration of the working mechanism of TENG in vertical contact-separation mode (a) before contact, (b) fully contact, the electric charges are generated due to contact electrification on PET and ZnO surfaces, (c) releasing, electrons flow between the electrodes, (d) fully released TENG in the electrical equilibrium state, no current flows, (e) further pressing, electrons flow in the reverse direction.



**Fig. 5.**  $V_{oc}$  of TENG device under switching polarity test of (a) acrylic support, (b) cardboard support, (c)  $I_{sc}$  of TENG device under switching polarity test, (d)  $V_{oc}$  and  $I_{sc}$  measured as a function of different load resistances, (e) instantaneous output power of the TENG device as a function of different load resistances, (f) TENG open-circuit voltage after rectification.

observed at  $26^\circ$  in Fig. 3(d) corresponds to the (1 0 0) plane of PET and is in good agreement with the published literature [43,44].

### 3.2. Working mechanism of TENG

The working mechanism of TENG is illustrated in Fig. 4. In this investigation, the TENG response was recorded in the vertical contact separation mode [16,45]. The TENG device is electrically neutral in the initial state because no charge is generated or inducted, with no electric potential difference between the two electrodes (Fig. 4(a)).

After applying an external mechanical pushing force, the PET surface contacts the bottom ZnO nanosheet film surface, and friction occurs between them. Due to the friction, electrostatic charges of opposite signs are generated and distributed on the two surfaces of the triboelectric layers, as shown in Fig. 4(b). Therefore, a potential difference can be established when the two contacted surfaces are separated. In order to screen this potential difference across the electrodes, instantaneous electrons flow across from the top electrode to the bottom electrode via the external load generating a voltage/current peak (Fig. 4(c)). Ultimately, equilibrium is reached when the two surfaces are completely separated, as shown in Fig. 4(d). As soon as the two surfaces are pressed together again, the electrostatically induced charges flow back through the external load to compensate for the electrical potential difference (Fig. 4(e)).

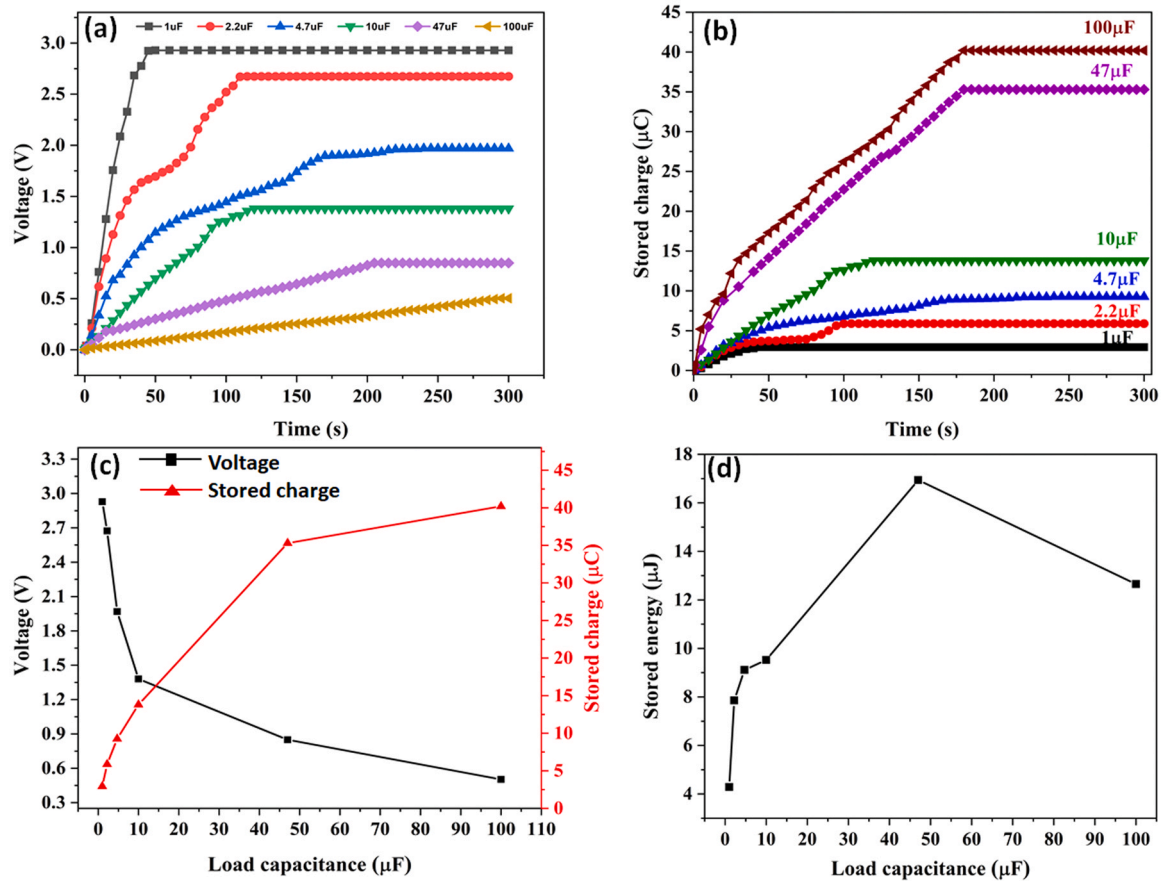
### 3.3. Performance analysis of TENG device

Fig. 5(a) shows the open-circuit voltage produced by the TENG device (size =  $5 \times 5 \text{ cm}^2$ , spacing = 1.2 cm) against repeated hand tapping under forward and reverse connections. TENG's forward and reverse connection geometry shows an average open-circuit voltage of  $\sim 4.9 \text{ V}$  (See SI video S1). The output voltage measurement when the connection to the oscilloscope is reversed is known as the switching polarity test. The switching polarity test verified that the voltage produced by TENG is not from any instrument noise and is

given by the TENG device only. In addition, the TENG response was recorded with and without anti-static gloves and confirmed that the contribution of static charge by hand is not there in the TENG output (SI, S4, video S2). To simplify the process and reduce costs, TENG was made with simple cardboard instead of acrylic sheets and tested its response against hand tapping, shown in Fig. 5(b) (SI, S5). TENG made with cardboard also showed a similar response as TENG made with acrylic sheets. The contribution of ZnO nanosheets piezoelectric output voltage was studied separately in piezoelectric device design and found  $\sim 300 \text{ mV}$  under the applied hand tapping pressures (SI, S6). The piezoelectric voltage generated from the ZnO is negligible when compared to the triboelectric output voltage of  $\sim 4900 \text{ mV}$ .

Further, TENG's short-circuit current ( $I_{sc}$ ) was measured under repeated hand tapping, and responses are shown in Fig. 5(c). The maximum value of  $I_{sc}$  is approximately  $10 \mu\text{A}$ , which is related to the transferred charges moving from one electrode to another under a short-circuit condition. Asymmetry in the positive and negative peaks (current/voltage) is attributed to the difference between the external force applied on the device and the restoring force of elastic spacers of the device [46–49]. The contact process is done by tapping force, whereas the separation process is due to the elasticity of spacers. Contact and separation process takes different time durations as results charge transfer rates will differ. This asymmetry in voltage and current signals are observed consistently in most literature reports, and more systematic study is required to explain the asymmetry. In conclusion, The  $V_{oc}$  and  $I_{sc} \sim 4.9 \text{ V}$  and  $10 \mu\text{A}$  were observed for the present TENG.

Further, electrical outputs ( $V_{oc}$ ,  $I_{sc}$ ) of the TENG device under different load resistances ( $R_L$ ) were recorded against hand tapping to find out the load characteristics and the instantaneous output power density of the TENG. The  $I_{sc}$  and  $V_{oc}$  of the TENG under the different loading resistance values in the range of  $50 \text{ k}\Omega$  to  $100 \text{ M}\Omega$  are shown in Fig. 5(d) (SI, S7). The  $V_{oc}$  increased with external load resistance and saturated at higher load resistance values greater than  $10 \text{ M}\Omega$  (SI S8). The saturated output voltage ( $\sim 4.5 \text{ V}$ ) is close to the open-circuit



**Fig. 6.** (a) Different load capacitors charging curves as a function of time, (b) stored charge curves of different load capacitors as a function of time (c) the charged voltage and stored charges as a function of load capacitance ( $C_L$ ) (d) the stored energy as a function of  $C_L$ .

voltage. At the same time, The  $I_{sc}$  decreases with increasing loading resistance due to Ohmic losses as expected. The load resistance dependency of  $V_{oc}$  and  $I_{sc}$  shows a trend similar to that described in the literature for other TENG's [50,51]. The TENG load resistance can be understood with a simple equivalent model proposed by Z L Wang and other research groups in the literature [52,53]. The TENG is equivalent to a variable capacitor connected to a voltage source (SI, S8). The voltage drops across the  $R_L$  increase until the optimum  $R_L$ , and saturate at the theoretically infinite load resistance comparable to open-circuit voltage [54].

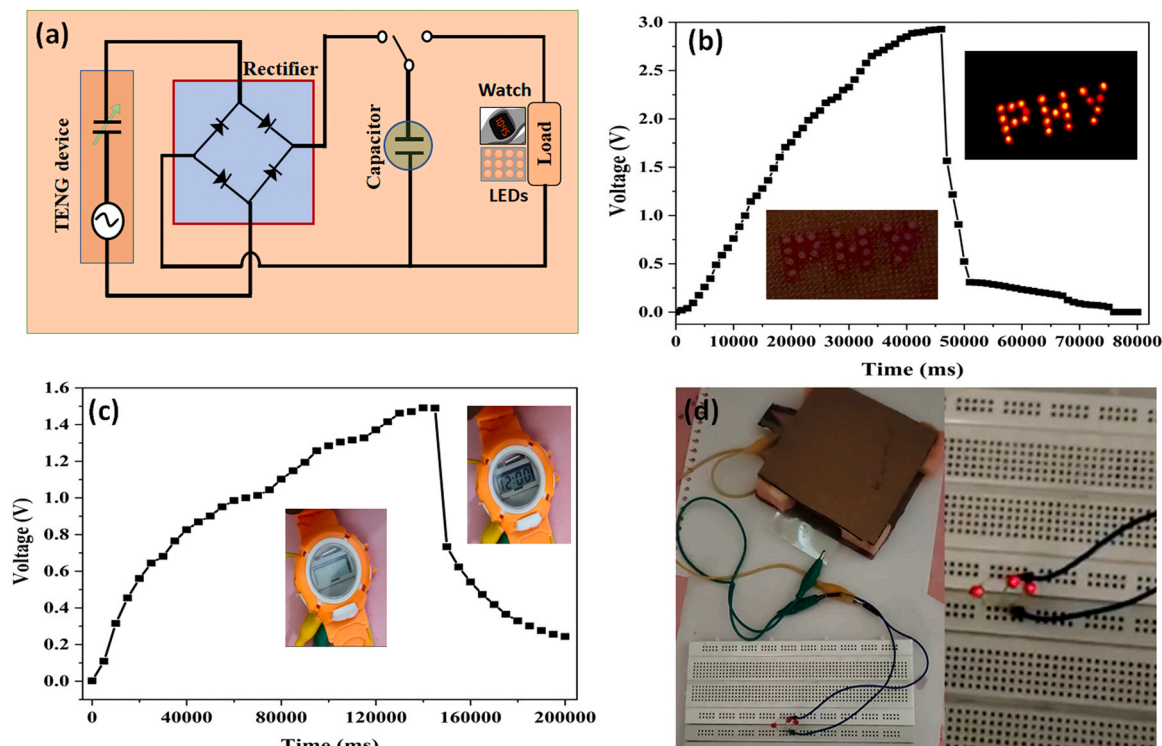
The TENG device's instantaneous output power ( $P = VI$ ) was calculated numerically with  $V_{oc}$ ,  $I_{sc}$  at different load resistance values and depicted in Fig. 5(e). The maximum instantaneous output power and power density of 25  $\mu\text{W}$  and 1  $\mu\text{W}/\text{cm}^2$  were observed at a load resistance value of  $\sim 5 \text{ M}\Omega$ . The maximum power transmission theorem can explain the nanogenerator's output power characteristics [55]. In the present report, instantaneous output power peaked under impedance matched conditions across a resistor  $\sim 5 \text{ M}\Omega$ . The output power decreased with the load resistance values greater than 5  $\text{M}\Omega$ . At higher load resistance, the output voltage got saturated as a result, the product ( $V_{oc} \times I_{sc}$ ) value decreased. The behavior of TENG devices under variable resistances illustrates a similar trend that has been described in the literature [56,57].

For practical applications, it is necessary to convert the TENG AC output into a DC output and store it in a capacitor or any energy storage element. The output voltage of the TENG device was rectified using a DB 107 IC rectifier to produce the DC voltage, and the DC output voltage graph is presented in Fig. 5(f). Further, the charging characteristics of various capacitors and the stored voltage, charge, energy as a function of the load capacitor were investigated. Fig. 6(a)

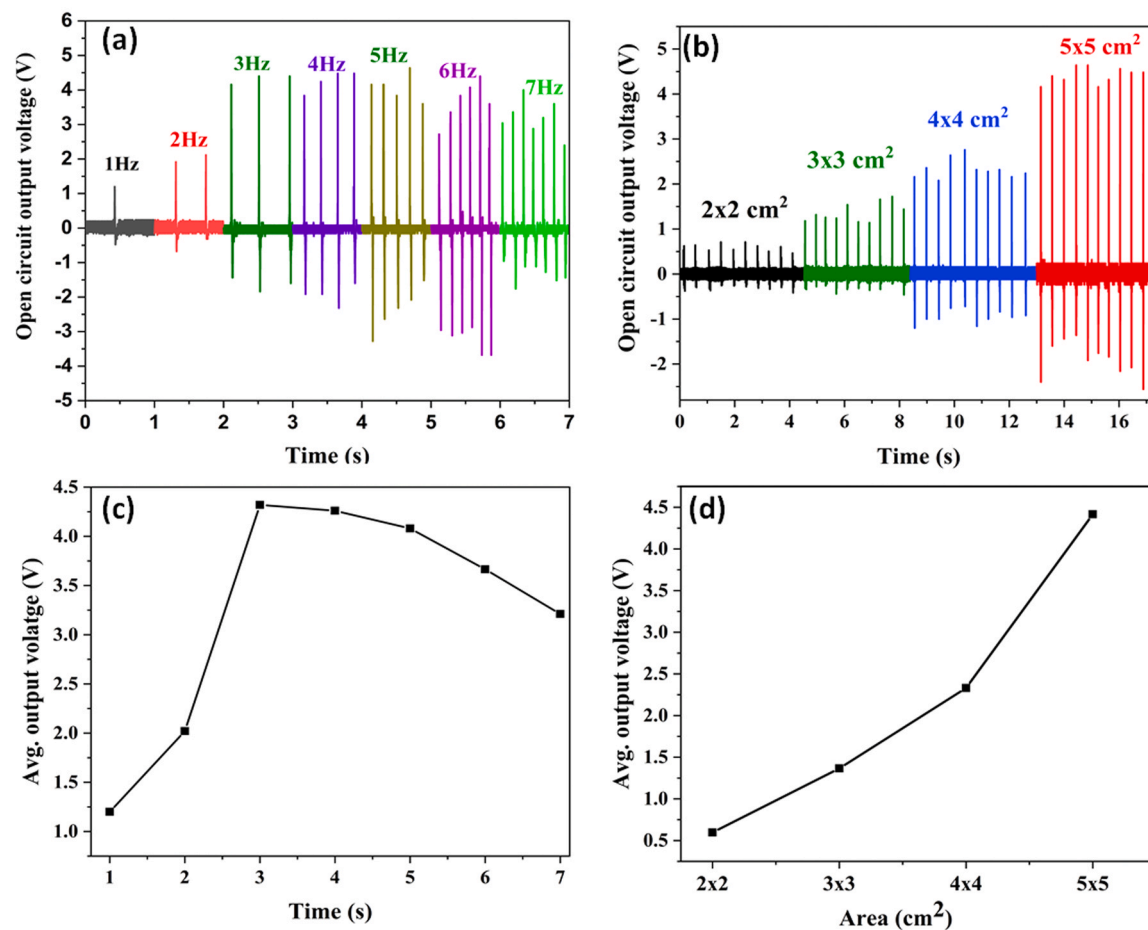
shows the charging voltages on different load capacitors ( $C_L$ ) of 1  $\mu\text{F}$ , 2.2  $\mu\text{F}$ , 4.7  $\mu\text{F}$ , 10  $\mu\text{F}$ , 47  $\mu\text{F}$ , and 100  $\mu\text{F}$ . The charging speed is greater for smaller  $C_L$ , and the time until the voltage is reached the saturation is shorter. The charge stored on these various capacitors was calculated by the product of the charged voltage (V) and capacitance  $C_L$ , as shown in Fig. 6(b). It is evident from Fig. 6(b) that an increment in the load capacitor value results in increased charge storage. The values of charged voltage and stored charge as a function of various load capacitance values were plotted as shown in Fig. 6(c). The behavior of charged voltage and stored charge with respect to the load capacitor is opposite. Fig. 6(d) illustrates the variation of the maximum stored energy as a function of the  $C_L$ . The maximum stored energy of 16.9  $\mu\text{J}$  was observed at the optimal  $C_L$  of 47  $\mu\text{F}$ . The behavior of TENG across different load capacitance values is similar to the reported literature [58,59].

Further, TENG was explored for powering digital watch, and 24 commercial LEDs with the help of 2.2  $\mu\text{F}$  and 1  $\mu\text{F}$  charged capacitors, respectively, as shown in Fig. 7(a). The charging and discharging curves of capacitors switching on digital watch and 24 LEDs are shown in Fig. 7(b)-(c). The inset of Fig. 7(b) and (c) shows photographs of the off and on status of the digital watch and LEDs (See SI, video S3,S4). Further, TENG can directly power up 3 LEDs continuously in response to hand tapping, as shown in Fig. 7(d) (See SI, video S5).

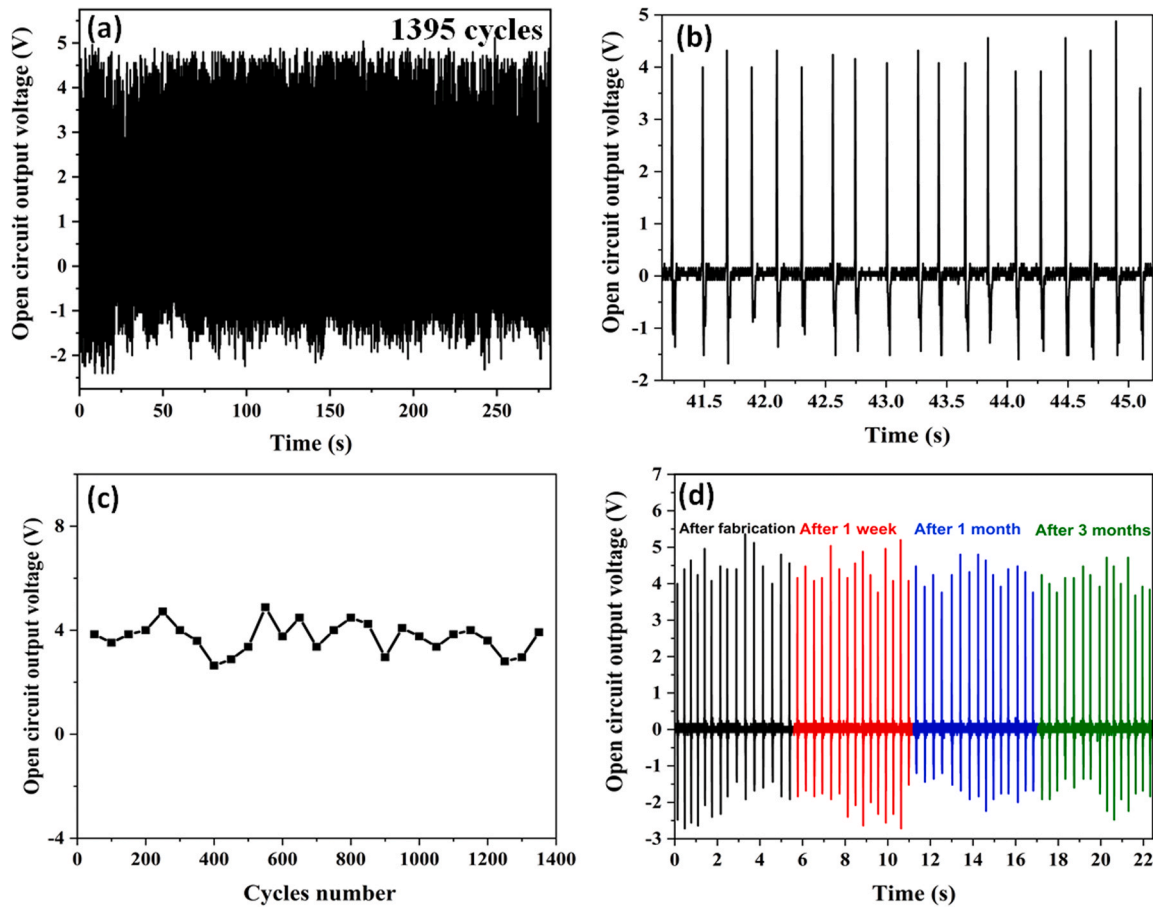
The  $V_{oc}$  of TENG was measured at different frequencies of hand tapping from 1 Hz to 7 Hz to study the frequency response. The response of TENG under different hand tapping frequencies is shown in Fig. 8(a). The average output voltage of the TENG increased with an increase in the frequency up to 4 Hz and decreased for later frequencies, as shown in Fig. 8(c). The increased output voltage with



**Fig. 7.** (a) Schematic connections for charging of capacitor using TENG and powering electronic devices, capacitor charging and discharging curves before and after power up the electronic devices (b) 24 red LEDs, (c) digital watch, (d) snapshot of the continuous switching on 3 LEDs under cyclic application of force.



**Fig. 8.** TENG output voltage as a function of (a) different frequency, (b) different area, variation of average output voltage with (c) different frequency, (d) different area.



**Fig. 9.** (a) TENG stability under 1395 cycles, (b) TENG response of some random cycles selected from the stability graph (c) every 50th cycle number output voltage values from the figure (a), (d) stability of the TENG at different time points.

increased frequency is due to the incomplete neutralization of charges [12,60]. The open-circuit voltage at high frequencies ( $> 4$  Hz) decreased. If the cycle of the compressive frequency is too high, the nanogenerator cannot return to the original position before the next force application results in a low output voltage [61,62].

The influence of triboelectric layer size (device size) on the TENG performance was studied. Fig. 8(b) shows the TENG response to hand tapping for various device dimensions of  $2 \times 2$ ,  $3 \times 3$ ,  $4 \times 4$ , and  $5 \times 5$  cm<sup>2</sup>. Fig. 8(d) clearly shows that the TENG average output voltage values were increased from 0.5 V to 4.5 V with an increase in device size. The increased active contact area of the triboelectric layers is responsible for improving the output voltage. A similar trend has also been reported for TENG's in the literature [63,64].

The stability and robustness of the TENG were studied to test the TENG for prolonging operation and practical applications. The TENG response was measured for 1395 external hand tapping force cycles, and the response is shown in Fig. 9(a). In the case of stability analysis, we took a gap of a few seconds for every 50–60 cycle's TENG response for applying the stable force by hand. In addition, we took a gap of a few seconds due to the oscilloscope display limitation. The TENG responses of such 50–60 cycles sets were merged to get the 1396 cycles, which is similar to the reported literature [64]. Fig. 9(a) shows that the fabricated TENG is highly stable, and a slight deviation in the output voltage was due to the variation in the manual hand tapping force and frequency. Fig. 9(b) shows the magnified view of some portion of the stability graph. Furthermore, the output voltage of the TENG was noted down for every 50th cycle (ex: 50, 100, 150 etc.) and plotted as shown in Fig. 9(c). Further, an in-house

developed tapping machine setup using a linear motor and sewing machine tested the TENG stability over many cycles ( $\sim 5000$  cycles) and found it stable (See, SI, S9, video S6, S7). Fig. 9(c) shows that an average output voltage value of  $\sim 4 \pm 0.5$  V was observed. Fig. 9(d) represents the TENG response at different times, for example, immediately after fabrication, one week, one month, and three months. The stable output response of the TENG was observed in all cases.

#### 4. Conclusion

In summary, triboelectric nanogenerator is fabricated with a new triboelectric pair and studied its characteristics. For the first time, the ZnO nanosheet film and the PET surface were acted as a friction layer for the triboelectric nanogenerator. The fabricated TENG operated in vertical-contact separation mode and produced an open-circuit voltage, short circuit current and instantaneous power density of  $\sim 4.9$  V,  $10 \mu\text{A}$  and  $1 \mu\text{W}/\text{cm}^2$ , respectively. The TENG can directly drive 3 LEDs simultaneously, and with the help of an energy storage element, it can switch on a digital watch and 24 LEDs. In addition, TENG shows exceptional structural durability and stability of electrical output over a large number of cycles. The TENG reported in this paper offers a simple design since no additional electrode deposition step is required and is cost-effective as ZnO nanosheets synthesis done by low-temperature hot plate assisted hydrothermal method. Furthermore, the TENG device fabrication can easily be scaled to large areas for higher performance. Therefore, fabricated TENG is a prospective candidate for self-powered sensors and devices.

# CRediT authorship contribution statement

**P. Supraja:** Investigation; Data curation, Writing – original draft, Software Methodology, Visualization, **R. Rakesh Kumar:** Conceptualization, Project administration, Supervision, Methodology, Formal analysis, Writing – original draft; Writing – review & editing, **P. Ravi Sankar:** Investigation; Software Methodology, Visualization, **D. Haranath:** Formal analysis, Project administration, Resources, Writing – review & editing, **K. Prakash:** Project administration, Resources, Formal analysis, Writing – review & editing, **Siju Mishra:** Investigation, Software Methodology, Visualization, **T. Venkatappa Rao:** Resources, Formal analysis, Writing – review & editing, **N. Jayarambabu:** Investigation; Data curation, **K. Uday Kumar:** Resources, Formal analysis.

# Declaration of Competing Interest

The authors declare that they have no known competing financial interests or personal relationships that could have appeared to influence the work reported in this paper.

# Acknowledgments

The authors are grateful to the Center for Advanced Materials (CAM) and Center for Automation and Instrumentation (CAI) for the microscope facility and X-ray diffraction facility, National Institute of Technology, Warangal.

# Appendix A. Supporting information

Supplementary data associated with this article can be found in the online version at [doi:10.1016/j.sna.2022.113368](https://doi.org/10.1016/j.sna.2022.113368).

# References

- A. Ahmed, I. Hassan, M.F. El-Kady, A. Radhi, C.K. Jeong, P.R. Selvaganapathy, J. Zu, S. Ren, Q. Wang, R.B. Kaner, Integrated triboelectric nanogenerators in the era of the internet of things, *Adv. Sci.* 6 (2019), <https://doi.org/10.1002/adv.201802230>
- J. Li, C. Wu, I. Dharmasena, X. Ni, Z. Wang, H. Shen, S.-L. Huang, W. Ding, Triboelectric nanogenerators enabled internet of things: a survey, *Intell. Conver. Netw.* 1 (2020) 115–141, <https://doi.org/10.23919/icn.2020.0008>
- I. Shabbir, N. Rubab, T.W. Kim, S.W. Kim, Healthcare management applications based on triboelectric nanogenerators, *APL Mater.* 9 (2021) 1–14, <https://doi.org/10.1063/5.0052605>
- X. Xia, Q. Liu, Y. Zhu, Y. Zi, Recent advances of triboelectric nanogenerator based applications in biomedical systems, *EcoMat* 2 (2020) 1–20, <https://doi.org/10.1002/eom.2.12049>
- R. Hinchet, W. Seung, S.W. Kim, Recent progress on flexible triboelectric nanogenerators for self-powered electronics, *ChemSusChem* 8 (2015) 2327–2344, <https://doi.org/10.1002/cssc.201403481>
- C. Wu, A.C. Wang, W. Ding, H. Guo, Z.L. Wang, Triboelectric nanogenerator: a foundation of the energy for the new era, *Adv. Energy Mater.* 9 (2019) 1–25, <https://doi.org/10.1002/aenm.201802906>
- D.W. Kim, J.H. Lee, J.K. Kim, U. Jeong, Material aspects of triboelectric energy generation and sensors, *NPG Asia Mater.* (2020), <https://doi.org/10.1038/s41427-019-0176-0>
- P. Bai, G. Zhu, Z.H. Lin, Q. Jing, J. Chen, G. Zhang, J. Ma, Z.L. Wang, Integrated multilayered triboelectric nanogenerator for harvesting biomechanical energy from human motions, *ACS Nano* 7 (2013) 3713–3719, <https://doi.org/10.1021/nn4007708>
- J. Zhong, Y. Zhang, Q. Zhong, Q. Hu, B. Hu, Z.L. Wang, J. Zhou, Fiber-based generator for wearable electronics and mobile medication, *ACS Nano* 8 (2014) 6273–6280, <https://doi.org/10.1021/nn501732z>
- Z. Zhao, L. Zhou, S. Li, D. Liu, Y. Li, Y. Gao, Y. Liu, Y. Dai, J. Wang, Z.L. Wang, Selection rules of triboelectric materials for direct-current triboelectric nanogenerator, *Nat. Commun.* 12 (2021) 1–8, <https://doi.org/10.1038/s41467-021-25046-z>
- Z.L. Wang, Triboelectric nanogenerators as new energy technology and self-powered sensors – principles, problems and perspectives, *Faraday Discuss.* 176 (2014) 447–458, <https://doi.org/10.1039/c4fd00159a>
- F.R. Fan, Z.Q. Tian, Z. Lin Wang, Flexible triboelectric generator, *Nano Energy* 1 (2012) 328–334, <https://doi.org/10.1016/j.nanoen.2012.01.004>
- S. Niu, Y. Liu, S. Wang, L. Lin, Y.S. Zhou, Y. Hu, Z.L. Wang, Theory of sliding-mode triboelectric nanogenerators, *Adv. Mater.* 25 (2013) 6184–6193, <https://doi.org/10.1002/adma.201302808>

- S. Niu, Y. Liu, S. Wang, L. Lin, Y.S. Zhou, Y. Hu, Z.L. Wang, Theoretical investigation and structural optimization of single-electrode triboelectric nanogenerators, *Adv. Funct. Mater.* 24 (2014) 3332–3340, <https://doi.org/10.1002/adfm.201303799>
- S. Niu, Y. Liu, X. Chen, S. Wang, Y.S. Zhou, L. Lin, Y. Xie, Z.L. Wang, Theory of freestanding triboelectric-layer-based nanogenerators, *Nano Energy* 12 (2015) 760–774, <https://doi.org/10.1016/j.nanoen.2015.01.013>
- S. Niu, S. Wang, L. Lin, Y. Liu, Y.S. Zhou, Y. Hu, Z.L. Wang, Theoretical study of contact-mode triboelectric nanogenerators as an effective power source, *Energy Environ. Sci.* 6 (2013) 3576–3583, <https://doi.org/10.1039/c3ee42571a>
- B. Yang, W. Zeng, Z.H. Peng, S.R. Liu, K. Chen, X.M. Tao, A. Fully, Verified theoretical analysis of contact-mode triboelectric nanogenerators as a wearable power source, *Adv. Energy Mater.* 6 (2016) 1–8, <https://doi.org/10.1002/aenm.201600505>
- H. Zhang, L. Quan, J. Chen, C. Xu, C. Zhang, S. Dong, C. Lü, J. Luo, A general optimization approach for contact-separation triboelectric nanogenerator, *Nano Energy* 56 (2019) 700–707, <https://doi.org/10.1016/j.nanoen.2018.11.062>
- R. Zhang, H. Olin, Material choices for triboelectric nanogenerators: a critical review, *EcoMat* 2 (2020) 1–13, <https://doi.org/10.1002/eom.2.12062>
- H. Yang, F.R. Fan, Y. Xi, W. Wu, Design and engineering of high-performance triboelectric nanogenerator for ubiquitous unattended devices, *EcoMat* 3 (2021) 1–36, <https://doi.org/10.1002/eom.2.12093>
- Z.L. Wang, Zinc oxide nanostructures: growth, properties and applications, *J. Phys. Condens. Matter* 16 (2004), <https://doi.org/10.1088/0953-8984/16/25/R01>
- D. Sakai, K. Nagashima, H. Yoshida, M. Kanai, Y. He, G. Zhang, X. Zhao, T. Takahashi, T. Yasui, T. Hosomi, Y. Uchida, S. Takeda, Y. Baba, T. Yanagida, Substantial narrowing on the width of “concentration window” of hydrothermal ZnO nanowires via ammonia addition, *Sci. Rep.* 9 (2019) 1–10, <https://doi.org/10.1038/s41598-019-50641-y>
- H. Qi, E.R. Glaser, J.D. Caldwell, S.M. Prokes, Growth of vertically aligned ZnO nanowire arrays using bilayered metal catalysts, *J. Nanomater.* 2012 (2012), <https://doi.org/10.1155/2012/260687>
- K.-H. Kim, B. Kumar, K.Y. Lee, H.-K. Park, J.-H. Lee, H.H. Lee, H. Jun, D. Lee, S.-W. Kim, Piezoelectric two-dimensional nanosheets/anionic layer heterojunction for efficient direct current power generation, *Sci. Rep.* 3 (2013) 2017, <https://doi.org/10.1038/srep02017>
- Y. Pyo, J. Hyeon, T. Whan, Highly-enhanced triboelectric nanogenerators based on zinc-oxide nanoripples acting as a triboelectric layer, *Appl. Surf. Sci.* 445 (2018) 50–55, <https://doi.org/10.1016/j.apsusc.2018.03.125>
- Y.P. Jeon, J.H. Park, T.W. Kim, Highly flexible triboelectric nanogenerators fabricated utilizing active layers with a ZnO nanostructure on polyethylene naphthalate substrates, *Appl. Surf. Sci.* 466 (2019) 210–214, <https://doi.org/10.1016/j.apsusc.2018.09.249>
- D. Li, C. Wu, L. Ruan, J. Wang, Z. Qiu, K. Wang, Y. Liu, Y. Zhang, T. Guo, J. Lin, T. Whan, Nano energy electron-transfer mechanisms for confirmation of contact-electrification in ZnO / polyimide-based triboelectric nanogenerators, *Nano Energy* 75 (2020) 104818, <https://doi.org/10.1016/j.nanoen.2020.104818>
- Y.P. Jeon, C. Wu, K.H. Yoo, T.W. Kim, Enhancement of the output voltage for triboelectric nanogenerators due to Al doping in the zinc oxide layer, *J. Alloy. Compd.* 831 (2020) 154913, <https://doi.org/10.1016/j.jallcom.2020.154913>
- S.N. Chen, C.H. Chen, Z.H. Lin, Y.H. Tsao, C.P. Liu, On enhancing capability of tribocharge transfer of ZnO nanorod arrays by Sb doping for anomalous output performance improvement of triboelectric nanogenerators, *Nano Energy* 45 (2018) 311–318, <https://doi.org/10.1016/j.nanoen.2018.01.013>
- W. Deng, B. Zhang, L. Jin, Y. Chen, W. Chu, H. Zhang, M. Zhu, W. Yang, Enhanced performance of ZnO microballoon arrays for a triboelectric nanogenerator, *Nanotechnology* 28 (2017) 135401, <https://doi.org/10.1088/1361-6528/aa5f34>
- Y.H. Ko, G. Nagaraju, S.H. Lee, J.S. Yu, PDMS-based triboelectric and transparent nanogenerators with ZnO nanorod arrays, *ACS Appl. Mater. Interfaces* 6 (2014) 6631–6637, <https://doi.org/10.1021/am5018072>
- X. Yue, Y. Xi, C. Hu, X. He, S. Dai, L. Cheng, G. Wang, Enhanced output-power of nanogenerator by modifying PDMS film with lateral ZnO nanotubes and Ag nanowires, *RSC Adv.* 5 (2015) 32566–32571, <https://doi.org/10.1039/c5ra02098k>
- A. Dos Santos, F. Sabino, A. Rovisco, P. Barquinha, H. Águas, E. Fortunato, R. Martins, R. Igreja, Optimization of ZnO nanorods concentration in a microstructured polymeric composite for nanogenerators, *Chemosensors* 9 (2021) 1–13, <https://doi.org/10.3390/chemosensors9020027>
- A.K. Gupta, C. Hsu, S. Lai, C. Lai, ZnO-polystyrene composite as efficient energy harvest for self-powered triboelectric nanogenerator, *ECS J. Solid State Sci. Technol.* 9 (11) (2020) 115019, <https://doi.org/10.1149/2162-8777/aba7fa>
- P. Supraja, R.K.R. Mishra S., D. Haranath, P.R. Sankar, K. Prakash, A simple and low-cost approach for the synthesis and fabrication of ZnO nanosheet-based nanogenerator for energy harvesting and sensing, *Eng. Res. Express* 3 (2021) 035022, <https://doi.org/10.1088/2631-8695/ac184b>
- S.S.K. Mallineni, H. Behlow, R. Podila, A.M. Rao, A low-cost approach for measuring electrical load currents in triboelectric nanogenerators, *Nanotechnol. Rev.* 7 (2018) 149–156, <https://doi.org/10.1515/ntrev-2017-0178>
- G. Min, A. Pullanchiyodan, A.S. Dahiya, E.S. Hosseini, Y. Xu, D.M. Mulvihill, R. Dahiya, Ferroelectric-assisted high-performance triboelectric nanogenerators based on electrospun P(VDF-TrFE) composite nanofibers with barium titanate nanofillers, *Nano Energy* 90 (2021) 106600, <https://doi.org/10.1016/j.nanoen.2021.106600>
- M.A. Jalili, Z. Khosroshahi, N.R. Kheirabadi, F. Karimzadeh, M.H. Enayati, Green triboelectric nanogenerator based on waste polymers for electrophoretic deposition of titania nanoparticles, *Nano Energy* 90 (2021) 106581, <https://doi.org/10.1016/j.nanoen.2021.106581>

- [39] A. Sharma, P. Agarwal, Triboelectric energy harvester performance enhanced by modifying the tribo-layer with cost-effective fabrication, *Mater. Res. Express* 6 (2019) 065514, <https://doi.org/10.1088/2053-1591/ab0f64>
- [40] N. Bi, L. Zhang, Q. Zheng, F. Zhuge, J. Li, X.P.A. Gao, J. Du, Control of ZnO nanowire growth and optical properties in a vapor deposition process, *J. Mater. Sci. Technol.* 33 (2017) 850–855, <https://doi.org/10.1016/j.jmst.2017.03.024>
- [41] V. Gaddam, R.R. Kumar, M. Parmar, G.R.K. Yaddanapudi, M.M. Nayak, K. Rajanna, Morphology controlled synthesis of Al doped ZnO nanosheets on Al alloy substrate by low-temperature solution growth method, *RSC Adv.* 5 (2015) 13519–13524, <https://doi.org/10.1039/c4ra14049d>
- [42] K.-H. Kim, B. Kumar, K.Y. Lee, H.-K. Park, J.-H. Lee, H.H. Lee, H. Jun, D. Lee, S.-W. Kim, Piezoelectric two-dimensional nanosheets/anionic layer heterojunction for efficient direct current power generation, *Sci. Rep.* 3 (2013) 2017, <https://doi.org/10.1038/srep02017>
- [43] Y.A. Stetsiv, M.M. Yatsyshyn, D. Nykpanchuk, S.A. Korniy, I. Saldan, O.V. Reshetnyak, T.J. Bednarchuk, Characterization of polyaniline thin films prepared on polyethylene terephthalate substrate, *Polym. Bull.* (2020), <https://doi.org/10.1007/s00289-020-03426-7>
- [44] C. Guillén, J. Herrero, Comparison study of ITO thin films deposited by sputtering at room temperature onto polymer and glass substrates, *Thin Solid Films* 480–481 (2005) 129–132, <https://doi.org/10.1016/j.tsf.2004.11.040>
- [45] Z.L. Wang, L. Lin, J. Chen, S. Niu, Y. Zi, Triboelectric Nanogenerator: Vertical Contact-Separation Mode, (2016) 23–47, [https://doi.org/10.1007/978-3-319-40039-6\\_2](https://doi.org/10.1007/978-3-319-40039-6_2)
- [46] S. Paria, R. Bera, S.K. Karan, A. Maitra, A.K. Das, S.K. Si, L. Halder, A. Bera, B.B. Khatua, Insight into cigarette wrapper and electroactive polymer based efficient TENG as biomechanical energy harvester for smart electronic applications, *ACS Appl. Energy Mater.* 1 (2018) 4963–4975, <https://doi.org/10.1021/acsaem.8b00951>
- [47] A. Ahmed, Design, Modelling and Analysis of Triboelectric Nanogenerators, (2018), [https://tspace.library.utoronto.ca/bitstream/1807/93154/1/Ahmed\\_Abdelsalam\\_E\\_201806\\_PhD\\_thesis.pdf](https://tspace.library.utoronto.ca/bitstream/1807/93154/1/Ahmed_Abdelsalam_E_201806_PhD_thesis.pdf)
- [48] M. Seol, J. Woo, D. Lee, H. Im, J. Hur, Y. Choi, Nature-replicated nano-in-micro structures for triboelectric energy harvesting, *Small* (2014) 3887–3894, <https://doi.org/10.1002/sml.201400863>
- [49] J. Chen, G. Zhu, W. Yang, Q. Jing, P. Bai, Y. Yang, T.C. Hou, Z.L. Wang, Harmonic-resonator-based triboelectric nanogenerator as a sustainable power source and a self-powered active vibration sensor, *Adv. Mater.* 25 (2013) 6094–6099, <https://doi.org/10.1002/adma.201302397>
- [50] J. Qian, X. Wu, D.S. Kim, D.W. Lee, Seesaw-structured triboelectric nanogenerator for scavenging electrical energy from rotational motion of mechanical systems, *Sens. Actuators A Phys.* 263 (2017) 600–609, <https://doi.org/10.1016/j.sna.2017.07.021>
- [51] I. Kim, H. Roh, J. Yu, H. Jeon, D. Kim, A triboelectric nanogenerator using silica-based powder for appropriate technology, *Sens. Actuators A Phys.* 280 (2018) 85–91, <https://doi.org/10.1016/j.sna.2018.07.013>
- [52] S. Niu, Z.L. Wang, Theoretical systems of triboelectric nanogenerators, *Nano Energy* 14 (2015) 161–192, <https://doi.org/10.1016/j.nanoen.2014.11.034>
- [53] C. Fang, T. Tong, T. Bu, Y. Cao, S. Xu, Y. Qi, C. Zhang, Overview of power management for triboelectric nanogenerators, *Adv. Intell. Syst.* 2 (2020), <https://doi.org/10.1002/aisy.201900129> (1900129).
- [54] S. Niu, Y.S. Zhou, S. Wang, Y. Liu, L. Lin, Y. Bando, Z.L. Wang, Simulation method for optimizing the performance of an integrated triboelectric nanogenerator energy harvesting system, *Nano Energy* 8 (2014) 150–156, <https://doi.org/10.1016/j.nanoen.2014.05.018>
- [55] J. Bird, *Electrical Circuit Theory and Technology*, 5th ed, Routledge, 2014, <https://doi.org/10.4324/9781315883342>
- [56] O. Access, Theoretical Prediction and Optimization Approach to Triboelectric Nanogenerator, (n.d.).
- [57] K. Xia, Z. Zhu, H. Zhang, Z. Xu, A triboelectric nanogenerator as self-powered temperature sensor based on PVDF and PTFE, *Appl. Phys. A Mater. Sci. Process.* 124 (2018) 1–7, <https://doi.org/10.1007/s00339-018-1942-5>
- [58] Y. Yao, T. Jiang, L. Zhang, X. Chen, Z. Gao, Z.L. Wang, Charging system optimization of triboelectric nanogenerator for water wave energy harvesting and storage, *ACS Appl. Mater. Interfaces* 8 (2016) 21398–21406, <https://doi.org/10.1021/acsami.6b07697>
- [59] S. Niu, Y. Liu, Y.S. Zhou, S. Wang, L. Lin, Z.L. Wang, Optimization of triboelectric nanogenerator charging systems for efficient energy harvesting and storage, *IEEE Trans. Electron Devices* 62 (2015) 641–647, <https://doi.org/10.1109/TED.2014.2377728>
- [60] Y.H. Ko, G. Nagaraju, S.H. Lee, J.S. Yu, PDMS-based triboelectric and transparent nanogenerators with ZnO nanorod arrays, *ACS Appl. Mater. Interfaces* 6 (2014) 6631–6637, <https://doi.org/10.1021/am5018072>
- [61] X.S. Zhang, M. Di Han, R.X. Wang, F.Y. Zhu, Z.H. Li, W. Wang, H.X. Zhang, Frequency-multiplication high-output triboelectric nanogenerator for sustainably powering biomedical microsystems, *Nano Lett.* 13 (2013) 1168–1172, <https://doi.org/10.1021/nl3045684>
- [62] C. Xue, J. Li, Q. Zhang, Z. Zhang, Z. Hai, L. Gao, R. Feng, J. Tang, J. Liu, W. Zhang, D. Sun, A novel arch-shape nanogenerator based on piezoelectric and triboelectric mechanism for mechanical energy harvesting, *Nanomaterials* 5 (2014) 36–46, <https://doi.org/10.3390/nano5010036>
- [63] Q. Wang, M. Chen, W. Li, Z. Li, Y. Chen, Y. Zhai, Size effect on the output of a miniaturized triboelectric nanogenerator based on superimposed electrode layers, *Nano Energy* 41 (2017) 128–138, <https://doi.org/10.1016/j.nanoen.2017.09.030>
- [64] T. Kamilya, P.K. Sarkar, S. Acharya, Unveiling peritoneum membrane for a robust triboelectric nanogenerator, *ACS Omega* 4 (2019) 17684–17690, <https://doi.org/10.1021/acsomega.9b01963>

**P. Supraja** received a Master's degree in Physics (Solid State Physics) in 2018 Kakatiya Government Degree College, Hanamkonda, Telangana, India. She joined NIT-Warangal in 2019 after clearing GATE. She is currently pursuing a Ph.D. degree in Physics Department at NIT-Warangal. Her current research interest includes energy harvesting, piezo and triboelectric nanogenerators.

**R. Rakesh Kumar** is working as an Assistant Professor, Department of Physics, National Institute of Technology-Warangal, and Telangana, India. He obtained his Ph.D. degree in Instrumentation and Applied Physics from the Indian Institute of Science (IISc) Bangalore, Karnataka, India. He has published more than 40 scientific papers so far in reputed journals. His current research interests are 2D materials, Energy harvesting, Energy storage, and Sensors.